



University of HUDDERSFIELD

University of Huddersfield Repository

Walton, Karl, Fleming, Leigh, Goodhand, Martin, Racasan, Radu and Zeng, Wenhan

High fidelity replication of surface texture and geometric form of a high aspect ratio aerodynamic test component

Original Citation

Walton, Karl, Fleming, Leigh, Goodhand, Martin, Racasan, Radu and Zeng, Wenhan (2016) High fidelity replication of surface texture and geometric form of a high aspect ratio aerodynamic test component. *Surface Topography: Metrology and Properties*, 4 (2). 025003. ISSN 2051-672X

This version is available at <http://eprints.hud.ac.uk/id/eprint/28048/>

The University Repository is a digital collection of the research output of the University, available on Open Access. Copyright and Moral Rights for the items on this site are retained by the individual author and/or other copyright owners. Users may access full items free of charge; copies of full text items generally can be reproduced, displayed or performed and given to third parties in any format or medium for personal research or study, educational or not-for-profit purposes without prior permission or charge, provided:

- The authors, title and full bibliographic details is credited in any copy;
- A hyperlink and/or URL is included for the original metadata page; and
- The content is not changed in any way.

For more information, including our policy and submission procedure, please contact the Repository Team at: E.mailbox@hud.ac.uk.

<http://eprints.hud.ac.uk/>

High fidelity replication of surface texture and geometric form of a high aspect ratio aerodynamic test component

This content has been downloaded from IOPscience. Please scroll down to see the full text.

2016 Surf. Topogr.: Metrol. Prop. 4 025003

(<http://iopscience.iop.org/2051-672X/4/2/025003>)

View [the table of contents for this issue](#), or go to the [journal homepage](#) for more

Download details:

IP Address: 161.112.232.103

This content was downloaded on 14/04/2016 at 11:25

Please note that [terms and conditions apply](#).

Surface Topography: Metrology and Properties



PAPER

High fidelity replication of surface texture and geometric form of a high aspect ratio aerodynamic test component

OPEN ACCESS

RECEIVED

9 December 2015

REVISED

20 January 2016

ACCEPTED FOR PUBLICATION

2 February 2016

PUBLISHED

4 April 2016

Karl Walton¹, Leigh Fleming¹, Martin Goodhand², Radu Racasan¹ and Wenhan Zeng¹

¹ EPSRC Centre for Innovative Manufacturing in Advanced Metrology, University of Huddersfield, Canalside East Building 3/04, Huddersfield, West Yorkshire HD1 3DH, UK

² Whittle Laboratory, University of Cambridge, 1 JJ Thomson Avenue, Cambridge CB3 0DY, UK

E-mail: k.walton@hud.ac.uk

Keywords: surface roughness replication, resin casting, infrared thermography, boundary layer transition, areal surface texture

Original content from this work may be used under the terms of the [Creative Commons Attribution 3.0 licence](https://creativecommons.org/licenses/by/4.0/).

Any further distribution of this work must maintain attribution to the author(s) and the title of the work, journal citation and DOI.



Abstract

This paper details, assesses and validates a technique for the replication of a titanium wind tunnel test aerofoil in polyurethane resin. Existing resin replication techniques are adapted to overcome the technical difficulties associated with casting a high aspect ratio component. The technique is shown to have high replication fidelity over all important length-scales. The blade chord was accurate to 0.02%, and the maximum blade thickness was accurate to 2.5%. Important spatial and amplitude areal surface texture parameter were accurate to within 2%. Compared to an existing similar system using correlation areal parameters the current technique is shown to have lower fidelity and this difference is discussed. The current technique was developed for the measurement of boundary layer flow 'laminar to turbulent' transition for gas turbine compressor blade profiles and this application is illustrated.

Nomenclature

Span	Aerofoil length parallel to the leading edge
Chord	Aerofoil width perpendicular to the leading edge
Reynolds number	A dimensionless number used to relate flow character similarity with variation in flow parameters (similarity parameter for flow viscosity)
Mach number	A dimensionless number used to relate flow character similarity with variation in flow parameters (similarity parameter for flow compressibility)

1. Introduction

Surface roughness and the associated drag on aero gas turbine components is a central consideration for design and in-service efficiency. The study of the influence of surface roughness on the flow over the

complex geometries of gas turbine compressor blade is relatively underdeveloped. The work detailed in this paper forms part of the wider effort to improve understanding of the influence of surface roughness in this context and particularly with respect to boundary layer transition.

1.1. Roughness induced drag and boundary layer transition

The region of flow over a aerofoil surface where viscous forces dominate is termed the boundary layer [1]. Increased skin friction and thus drag due to surface roughness is determined by the roughness character and the nature of the boundary layer. A 'laminar' boundary layer is associated with low drag which increases as transition to the 'turbulent' flow regime occurs, though a 'laminar (viscous) sub layer' always persists close to the surface. Surface roughness is one factor that can influence (laminar-turbulent) 'transition' though there is no reliable method of predicting it. In addition to increasing drag by causing transition, roughness asperities that project through the laminar sub-layer cause a direct increase in drag by the formation of eddies. This effect increases momentum transfer from the surface to the turbulent boundary layer increasing its magnitude which is often referred

to as ‘thickening of the turbulent boundary layer’. When this mechanism is preceded by roughness induced transition this is described as ‘premature transition’. Thus roughness induced drag is limited to these two different and physically distinct mechanisms and when neither is acting, a surface is said to have ‘admissible’ roughness or to be ‘hydraulically smooth’. It is important to distinguish between these drag rise mechanisms as premature transition cannot be accounted for in existing models of roughness induced drag. No single test method is available to measure roughness induced drag and distinguish which initial ‘drag rise mechanism’ is at play. Roughness induced drag is measured directly by the momentum loss wind tunnel technique [2], but to identify possible premature transition an infrared thermographic technique must be used. In a high speed wind tunnel the temperature the boundary layer of a test surface has a higher temperature than the bulk flow. Due to the their differing flow character the turbulent boundary layer is seen to be hotter than the laminar boundary layer, thus the transition is visible in the infrared. This technique is only suitable for thermally insulating surfaces [3] as metals disperse heat too quickly to sustain an adequate temperature gradient for current thermal cameras to capture. The solution to this problem, described in the current paper is the manufacture of a facsimile of the titanium test aerofoil in a thermally insulating polyurethane resin.

1.2. Areal surface metrology and replication fidelity

High fidelity replication of surface roughness has long been practiced in the field of surface metrology to allow the measurement of surfaces not easily accessed directly, or for surface archiving. Hansen *et al* and Nilsson and Ohlsson [4, 5] report areal parametric comparison results form a range of rigid thermosetting polymers and silicone elastomer. They report typical figures of 10% variation in (Sa, Sz, Vmp, Vvc, Vvv) for single stage replication of machines surfaces with an approximate Sa range of 0.2–1.7 μm . However warping and shrinkage due to heat generated during curing make most of these dedicated roughness replication resin options inappropriate for a precision casting application. More recently Song *et al* [6] applied the normalized cross-correlation function (CCF) in this context, the CCF is the sum of the product of the point heights of two superimposed areal surface measurements. CCF_{max} is then the maximum value for this function when the master (M) and replica (R) measurement fields are optimally aligned. Thus two identical surfaces perfectly aligned would give a CCF_{max} value of 100%. However, they note this parameter ‘is not sensitive to a difference in the relative scale of surface heights between topographies of similar shape’. To mitigate this limitation they offer a second metric called the topography difference parameter D_s .

Where

$$D_s = \text{Sq}^2_{(M-R)} / \text{Sq}^2_{(M)}. \quad (1)$$

A ‘difference’ surface is formed by subtracting the replica surface from master surface at the optimal cross correlation position from above. The square of the rms roughness of this difference surface is then divided by the square of the rms roughness of the master surface to give the difference parameter. Thus two identical surfaces perfectly aligned would give a D_s value of 0%. Unlike CCF_{max} this parameter is sensitive to scale variations. Both of these parameters are expressed in percentage terms.

A replication technique similar to the one developed in the current paper is reported by Koch and Katterwe [7]. They use the well-established two stage casting method; a flexible female impression of the master is taken in silicone elastomer, epoxy resin is vacuum cast into this mould to form the replica. Vacuum casting as detailed by Akevali [8] is used to degas resin to avoid bubbles compromising surface replication quality. Koch and Katterwe [7] applied their technique to the replication of bullets for forensic purposes and have a patent application for that purpose [9]. This technique was assessed using the CCF_{max} and D_s metrics by Song *et al* [10]. They report mean values of CCF_{max} and D_s as favourable as 99% and 1% respectively.

Bergstrom *et al* [11] also used the idea of correlating by plotting the point heights of master and replica surfaces against each other. Thus, deviation of regression line gradient and coefficient of determination (R^2) from their ideal values of unity for these plots become useful metrics for replication fidelity. In addition trends in the distribution of these correlation plots can give meaningful information about the nature of errors in replication fidelity, though they report no replication results using their techniques.

1.2.1. Objectives

In the present paper the primary objectives are to:

Demonstrate a method for precision replication of both geometry and surface texture of a high aspect ratio test aerofoil in polyurethane resin. Use a full range of current surface and geometry comparison techniques to assess replication fidelity. Validate replication fidelity by direct aerodynamic drag comparison. Illustrate the aerodynamic application of the technique to measure boundary layer transition on rough test aerofoils using infrared thermography.

2. Materials and methods

2.1. Replication resins

In the first stage of replication MicrosetTM was used it is a proprietary highly elastic synthetic rubber replication compound developed for and well proven in the replication of surface roughness detail [5], with faithful

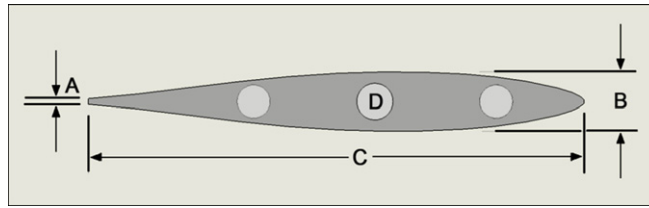


Figure 1. Cross section of the test aerofoil. Showing: (A) trailing edge thickness 0.5 mm, (B) maximum thickness 5.5 mm, (C) width of 45 mm, (D) mounting and registration points. The aerofoil has a uniform cross section along its 118 mm length.

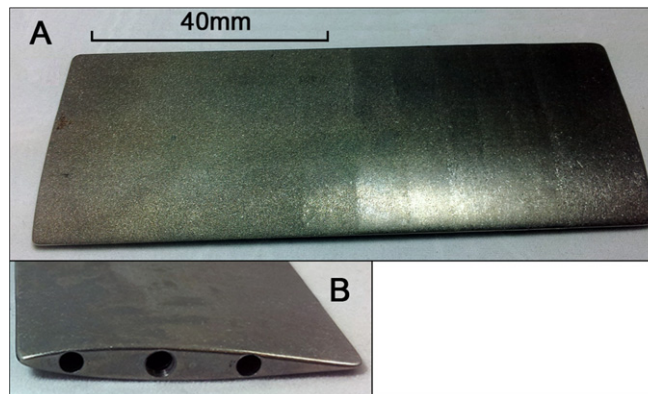


Figure 2. Titanium test aerofoil T1, showing (A) the incremental test surface roughness regions (B) profile; mounting points and registration points.

replication claimed to length scales to $0.1 \mu\text{m}$ [12]. It has been shown that for similar applications Microset™ leaves no significant surface residue [13], and is dimensionally stable when cured.

In the second replication stage a two part thermo-setting polyurethane casting resin was used; polyol (monomer) and isocyanate polymerising catalyst are mixed in equal quantities. The mixture has a viscosity and density close to that of water and cures with a claimed linear shrinkage of approximately 0.2% [14].

2.2. Test aerofoils

Figure 1 shows a cross section of the test aerofoil, the profile of which is designed to simulate the flow conditions over a typical aero gas turbine compressor blade. The trailing edge section (A) has an aspect ratio of approximately 1:200. This slender character posed significant technical challenges in achieving high fidelity replication of both geometric form and surface roughness in the casting process. The test surfaces of the replicated aerofoil must be unmarked by mould parting lines or casting runners and risers, thus access for mould filling is limited.

Two titanium aerofoils (T1 and T2) were manufactured; T2 was shot blasted and then incrementally polished by a mass finishing process. At each polishing increment the aerofoil was wind tunnel tested to measure the drag induced by the surface roughness compared to the hydraulically smooth case. The second aerofoil T1 seen in figure 2 was suitably masked and

processed in parallel with T2 to capture the eight incrementally textured test surfaces. Aerofoil T1 was replicated in polyurethane resin to give aerofoil R1 (Replica or Resin 1).

Separate aerofoils were used for drag and surface texture assessment for logistical reasons as the two processes were carried out at separate locations.

2.3. Aerofoil replication

2.3.1. Stage one

Figure 3 shows the open empty replica casting box in which the two stage replication procedure was carried out.

Figure 4 shows a sample titanium aerofoil mounted in the casting box and figure 5 shows the casting box assembled ready for first stage filling. Microset™ [12] silicone elastomer was injected via the two nozzles (C), until the riser tubes (B) were both approximately half filled with elastomer. The filler holes were plugged and the casting box transferred to a compressed air pressure vessel and allowed to cure for 24 h at approximately 50 psi. The ends of the casting box were then removed and the remaining bolts slackened to allow the titanium aerofoil to be extracted.

2.3.2. Stage two

The mould void was then filled from the top with polyurethane resin [14] via new sprue and riser tube (figure 5(B)). The casting box was then returned to the pressure vessel to cure for 24 h and the same pressure

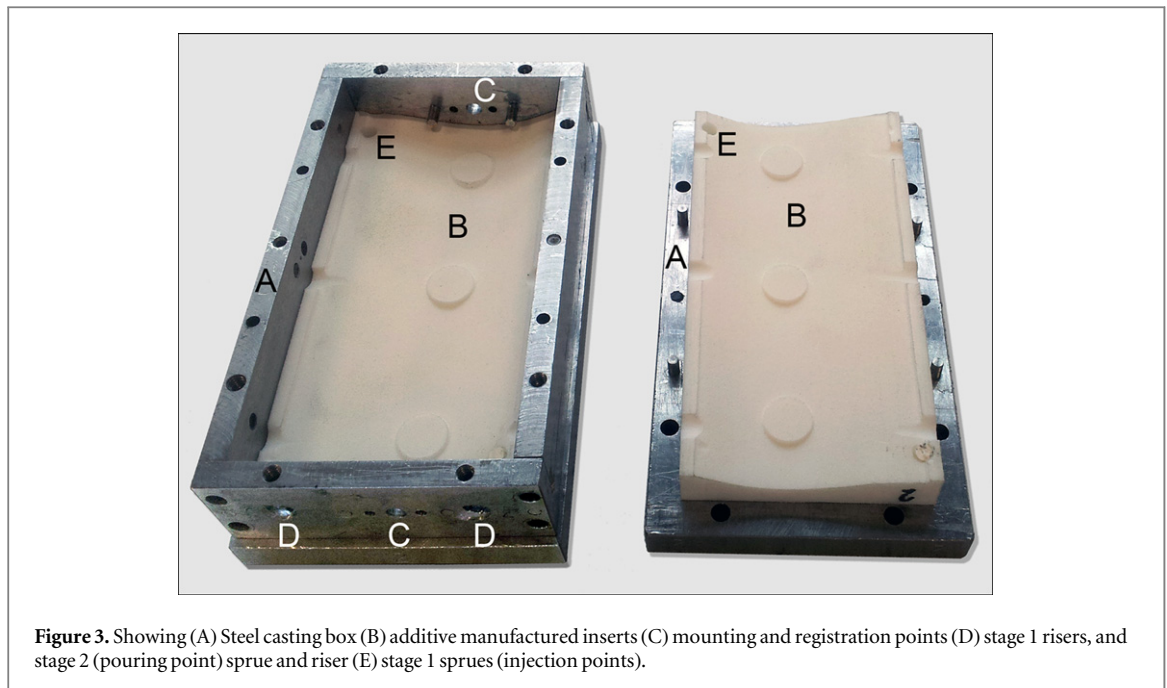


Figure 3. Showing (A) Steel casting box (B) additive manufactured inserts (C) mounting and registration points (D) stage 1 risers, and stage 2 (pouring point) sprue and riser (E) stage 1 sprues (injection points).

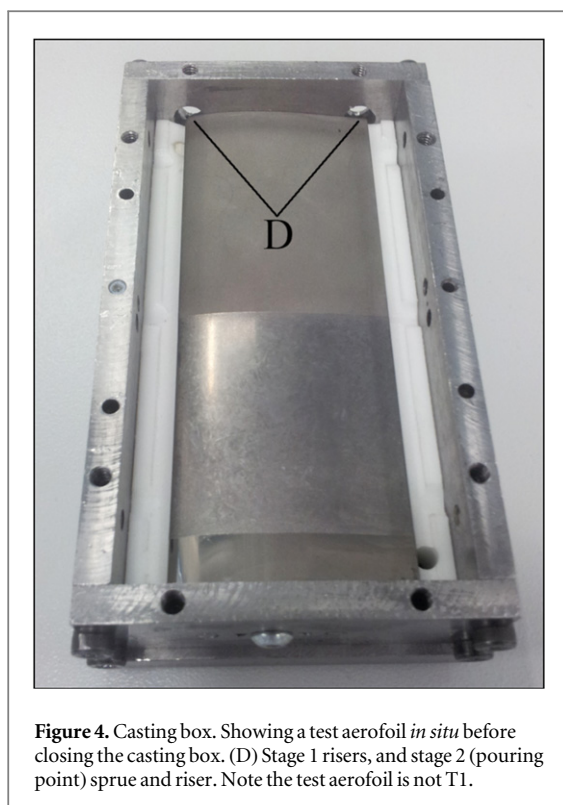


Figure 4. Casting box. Showing a test aerofoil *in situ* before closing the casting box. (D) Stage 1 risers, and stage 2 (pouring point) sprue and riser. Note the test aerofoil is not T1.

recorded from stage one. The replication process is summarised schematically in figure 6.

2.4. Replication fidelity

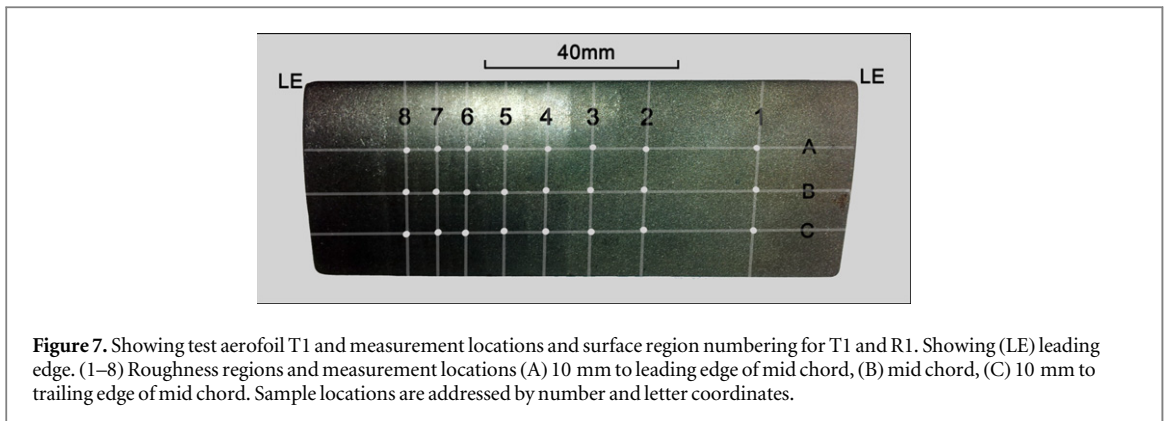
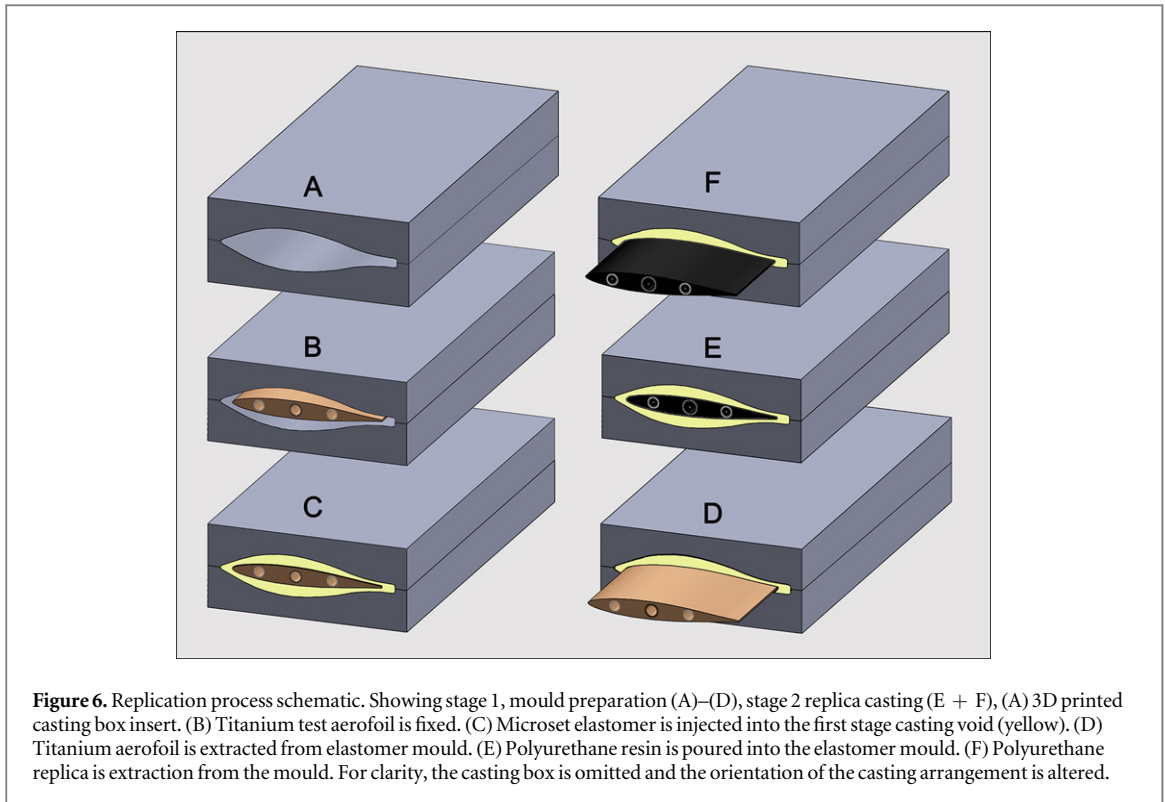
2.4.1. Surface metrology

A focus variation (FV) instrument (Alicona IFM G4) [15] was used to assess surface topography with; 20× microscopic objective, 2.9 μm lateral resolution (approximately 1 μm sample spacing) and 60 nm vertical quantisation and automatic field stitching. T1 and R1 surfaces were characterised (see figure 7) in



Figure 5. Casting box. Showing arrangement for injection of microset. (A) Casting box (B) risers for microset, and sprue and riser for PU pouring (C) injection points (sprues) for Microset.

fields of 1 × 1.3 mm at locations spaced centrally to the roughness bands along three spanwise lines, one central to the chord and one approximately 10 mm to both the leading and trailing edges of this line, 48 fields in all. To ensure optimal alignment for comparison purposes these sample fields were precisely located with the use of a mounting jig and specific surface



topography landmarks. Final adjustment and alignment was done by overlaying microscopic field images in a suitable graphics package and then cropping the point height maps to match. For each measurement field the Alicona captures a full colour image at the same resolution as the point height map. This alignment and cropping process required the use of a dedicated routine written in Alicona's scripting language. The acquired data was processed using the Alicona's proprietary algorithms via scripting language. A second order polynomial surface was fitted to and removed from the data sets to eliminate the aerofoil geometry, followed by a Gaussian 'S filter' (short wavelength noise filter) of 0.004 mm wavelength. A long wavelength 'L filter' [16] was not applied as all longer surface wavelengths were to be considered in the surface replication comparison. The point height correlation plot method was used to compare the results for regions A1, A4, and A8. Sample

locations A, B and C, 1 through 6 were compared directly using the areal surface parameters S_q , S_{sk} and Sal . S_q (μm); the rms height and the standard deviation of the point height distribution for the surface. $S_{sk}(-)$; skewness of the surface height distribution or the extent to which it is dominated by peaks or pits [17, 18]. Sal (μm); fastest decay autocorrelation length [17, 18] and a measure of the spatial (lateral) scales of surface topography. Taken together these parameters represent a good description of surface texture character for comparative purposes.

For a single relocated sample fields (not listed in figure 7 approximately 1×1 mm) in each of the hydraulically rough regions (1–5) of T1 and R1 the fidelity parameters CCF_{max} and D_s were calculated and compared. Five repeated replications of R1 were cast and the repeatability of the process was analysed for the measurement field in region 4.

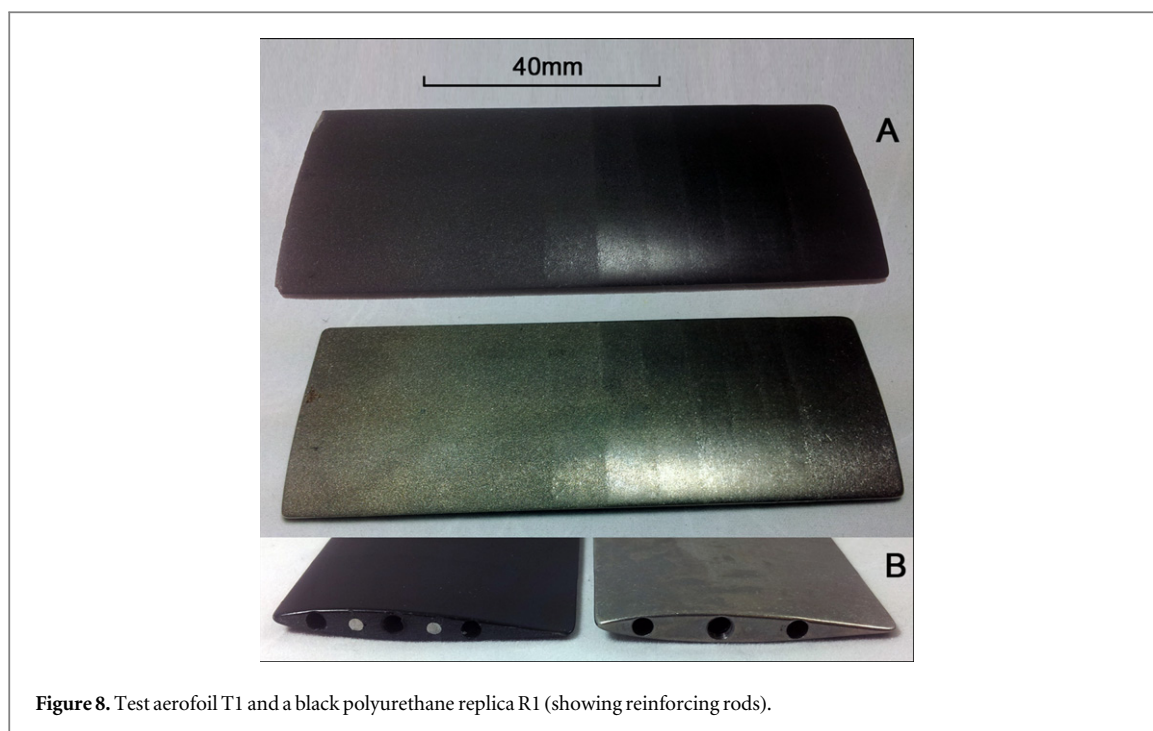


Figure 8. Test aerofoil T1 and a black polyurethane replica R1 (showing reinforcing rods).

2.4.2. Aerofoil geometry and drag validation

A half rough, half hydraulically smooth Titanium test aerofoil (see figure 4) and its replica were prepared to assess replication geometry fidelity using the gomTM [19] optical 3D coordinate measurement system. In addition a wind tunnel method was used to compare the aerodynamic drag losses of the test aerofoils. This drag testing was carried out in a transonic type wind tunnel with a range of continuous flows over Mach number (M) 0–1 and Reynolds (Re) $0.1-1 \times 10^6$.

2.5. Aerodynamic application

An infrared camera FLIR A315 [20] was used in combination with the wind tunnel described in section 0 to investigate the influence of surface roughness on boundary layer transition on the test aerofoil R1.

3. Results

3.1. Replication

Figure 8 shows the black polyurethane replica test aerofoil R1 produced by the technique detailed in the current work and the titanium test aerofoil T1.

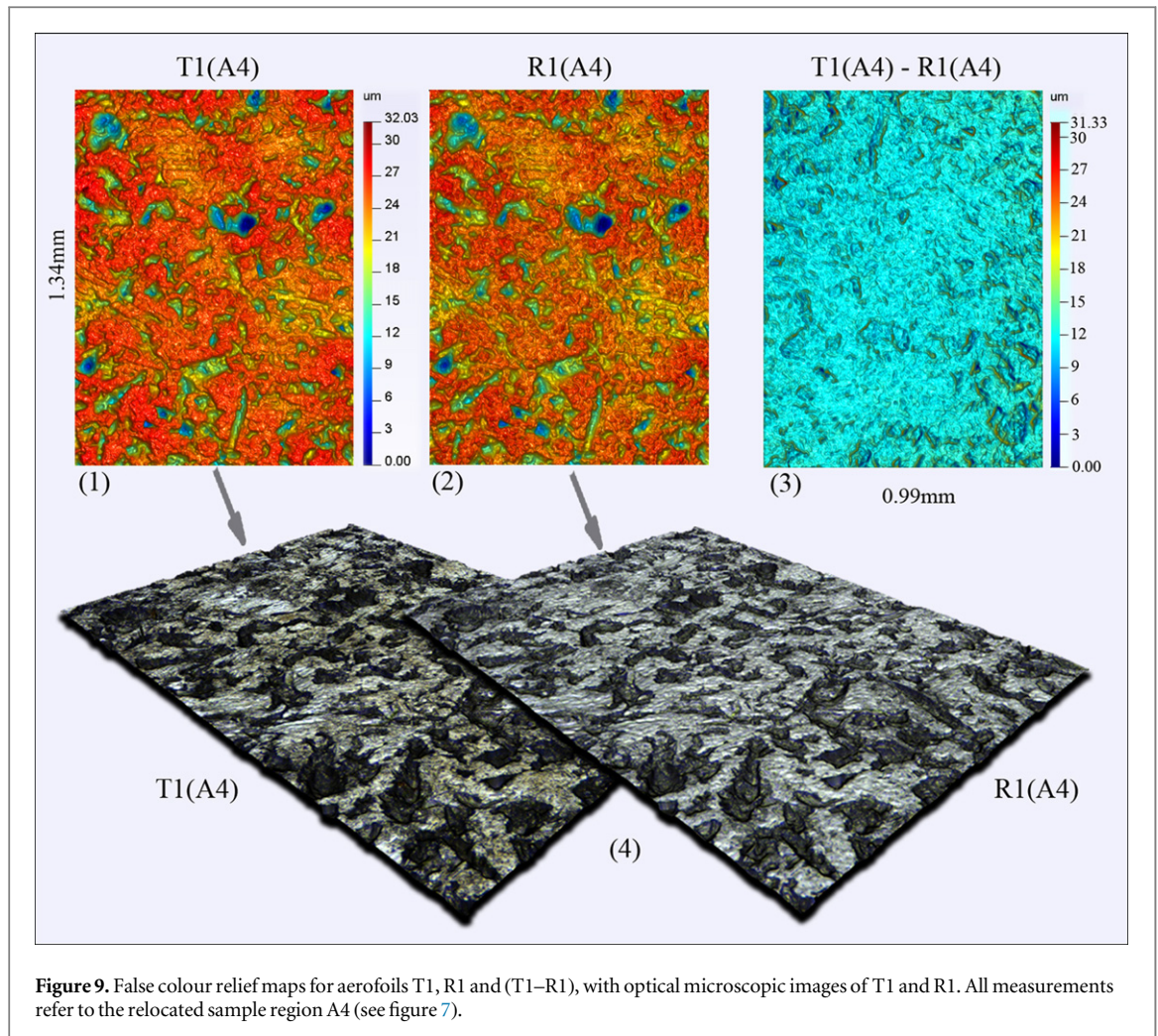
3.2. Replicated surface metrology

Within the range of the wind tunnel test conditions regions 6, 7 and 8 of the test aerofoils were determined to be hydraulically smooth, i.e. their surface roughness had no influence on flow. Thus the regions having roughness levels equal to or lower than region 6 are not considered for the current aerodynamic application but are included in the assessment of the replication process fidelity. A small number of optical spike artefacts were seen in some of the sample fields

for T1 but were absent from R1. Such spikes are characteristic of the use of a FV instrument on a surface having localised regions of low surface micro-texture. Crystalline blast media being retained in the surface or localised high polish are likely causes of low micro-texture. These spikes were hand cropped from the surface to the median value of the surrounding surface. They are inherently high aspect ratio and can increase extreme surface parameters by up to 100%, though S_q , S_{sk} , S_{al} are typically affected by less than 1%. Removal was limited to spikes greater than approximately 20% of the nominal surface height. However, remaining artefacts of this type are considered as a possible source of reduced fidelity in the correlation parameters. Figures 9(1) and (2) show false colour relief maps of region A4 on aerofoils T1 and R1 these give a visual indication of the overall replication and repositioning fidelity. Figure 9(3) shows the false colour relief map of the data set gained by subtracting the point heights of (2) from (1) this is an example of the (M–R) ‘master—replica’ surface referenced in equation (1).

A significant proportion of this ‘difference map’ is close to an ideal uniform plane that would represent perfect replication the remaining pits and peaks thus represent replication and alignment errors. Figure 9(4) shows optical micrographs of region A4 on aerofoils T1 and R1, the same region seen in figures 9(1), (2) and (3).

The polished plateau regions of the replicated surfaces in figure 9 (R1(A4)) show evidence of a replication artefact in the form of small scale surface texture not present in the original surfaces. Figures 10(a)–(c) show point height correlation plots of region A1, A4, and A8 respectively for aerofoils T1 and R1.

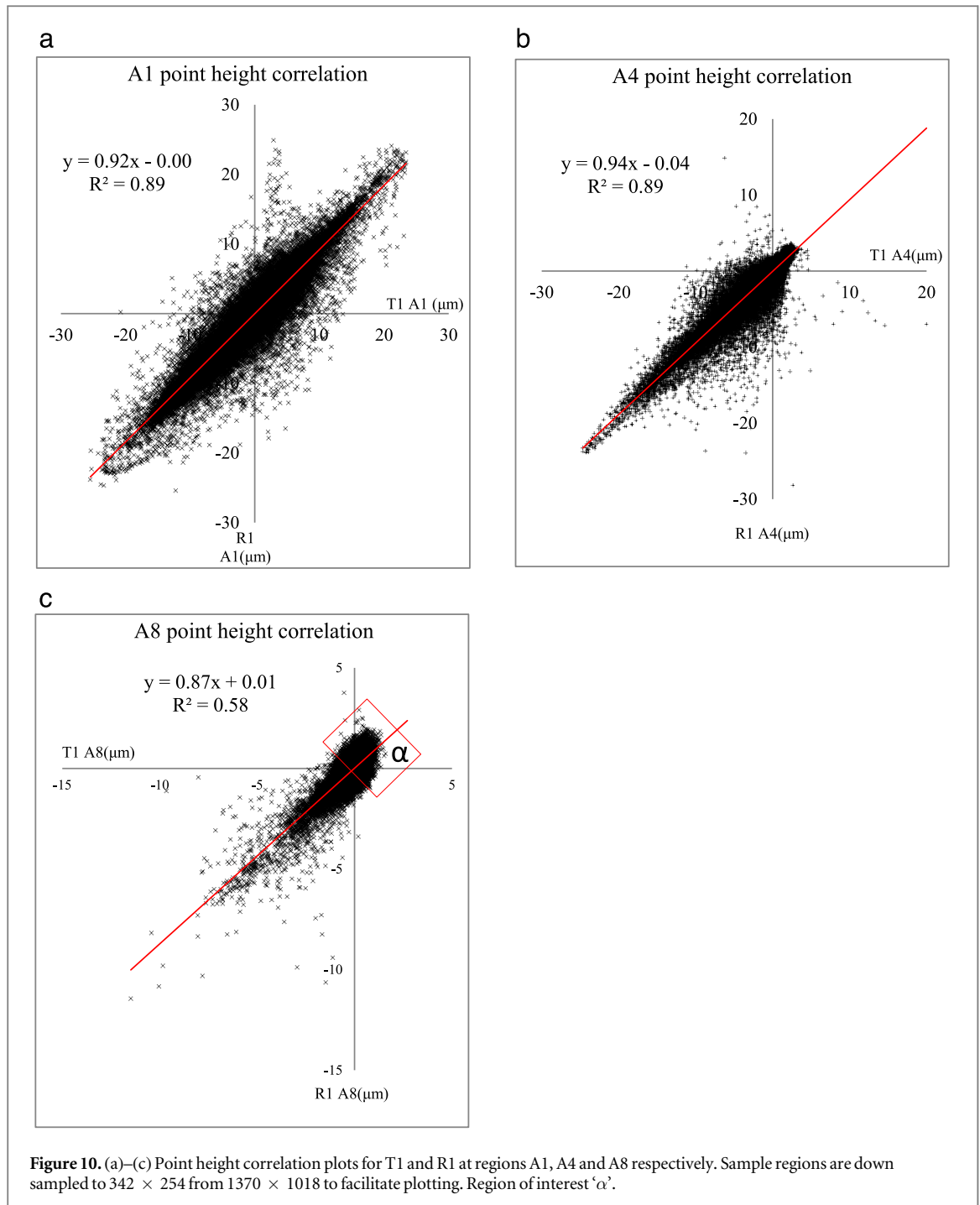


The replication artefact noted in region A4 has little impact on the overall character of the surface. However, as the vertical range of the surface decreases and the plateau regions become predominant at high levels of polish the artefact becomes a significant component of the surface texture. This trend of decreasing replication fidelity is illustrated in the R^2 values of regions A1 to A4 to A8 in figure 10. For region A8 the area of the correlation plot corresponding to the highest points on the surface (region ‘ α ’) shows significant distortion. This generalised shifting of points height correlations toward the ‘replica’ axis illustrates the dominance of this small scale texture on the increasingly ‘plateau like’ surface.

The influence of this textural artefact is also clear in the areal parametric analysis of the replication technique. Peak material volume (V_{mp}) and reduced peak height (S_{pk}) both reflect the specific character of this surface portion and for sample locations A5 and A6 (see figure 7) varied by as much as 30%. However, variations in the key areal parameters S_q , S_{al} and S_{sk} in table 1 between T1 and R1 were seen to be relatively small and approximately uniform with region. The mean and standard deviation for these parameters for regions 1 through 6 are shown in table 1. Overall vertical and lateral scale replication fidelity is high as illustrated by the

small mean difference in S_q and S_{al} respectively in table 1. Significantly poorer fidelity is indicated by the variation in skewness (S_{sk}) of the replicated surfaces, though this is to be expected as S_{sk} is sensitive to surface outliers, as it is the third (cubic) moment of the surface height distribution. The mean and standard deviation of the regional percentage differences in parameter are quoted to give an overall impression of the fidelity of replication and its variance. The hydraulically smooth surfaces of regions 7 and 8 (S_q values of approximately $1 \mu\text{m}$) showed a 15%–20% increase in S_q values with replication, though the overall trend of decreasing roughness with region was unaltered. A negative correlation between surface polish and replication fidelity is also seen in [21], though the surfaces are significantly less rough than those in the current study. The cause of this loss of fidelity on increasingly smooth surfaces is not clear, though it is possible that heat evolved during curing may influence this.

Table 2 shows the fidelity (regions 1–5) and repeatability data (region 4) using parameters CCF_{max} and D_s . Individual region values are not quoted for fidelity as they were approximately constant across the regions. For the repeatability study the sample field in region 4 was measured on five different replicas of T1 (5 versions of R1).



The mean region fidelity figures indicates adequate replication quality, though they are somewhat poorer than the optimised values of 99% and 1% reported in [10]. Values of D_s show a significantly larger range than do the values of CCF_{\max} . This discrepancy in the variance of these parameters may indicate a variation in scale changes due to shrinkage across the samples. The data in table 2 also indicates that the current replication technique offers similar levels of fidelity (accuracy) and repeatability (precision).

3.3. Replicated aerofoil geometry

Optical coordinate scanner point cloud data sets for the master and replica aerofoils were aligned by least

square best fit using CatiaTM [22]. For this fitting, figure 11 shows the discrepancy map for the dimensions of the replica with respect to the master, the two sides of the aerofoil map are shown unfolded along the leading edge. The contours appear to indicate a warping discrepancy, as diagonally opposite corners (A) and (B) show opposite discrepancies to (A*) and (B*) on opposite sides of the map. The corner A, A* being at the leading edge of the test aerofoil and B, B* at the trailing edge. Warping is to some extent mitigated by the socket type mounting of both ends of the aerofoil into the wind tunnel rig. The scale indicates that approximately 90% of the fitted points

Table 1. Shows values for the three locations A, B, C in regions 1–6 on the master and replica aerofoils T1 and R1 (see figure 7 for details) for parameters Sq, Sal and Ssk, and their mean values the percentage difference of these mean parameters for each region of R1 compared to T1, in addition to the mean and standard deviation of the percentage differences of the means.

Location	Parameter	Sq (μm)		Sal (μm)		Ssk (\AA)	
		T1	R1	T1	R1	T1	R1
1	A	5.49	5.34	38.10	38.20	-0.20	-0.18
	B	4.99	4.81	37.00	36.70	-0.53	-0.49
	C	5.75	5.56	40.00	39.60	-0.39	-0.41
	Mean	5.41 ^a	5.24	38.37	38.17	-0.38	-0.36
	% diff of means	3.23		0.52		4.62	
2	A	6.47	6.28	38.80	39.00	-0.43	-0.40
	B	5.80	5.68	36.10	35.90	-0.30	-0.27
	C	6.07	5.88	40.70	41.50	-0.52	-0.49
	Mean	6.11 ^a	5.95	38.53	38.80	-0.42	-0.39
	% diff of means	2.72		-0.69		7.47	
3	A	5.85	5.68	36.20	36.40	-0.64	-0.58
	B	5.74	5.57	40.30	40.40	-0.79	-0.71
	C	5.42	5.22	38.90	39.90	-0.78	-0.76
	Mean	5.67	5.49	38.47	38.90	-0.74	-0.68
	% diff of means	3.16		-1.13		7.55	
4	A	3.48	3.45	36.70	36.40	-2.19	-1.95
	B	4.02	3.95	39.70	39.40	-1.64	-1.55
	C	3.94	3.89	37.70	37.40	-1.80	-1.65
	Mean	3.82	3.76	38.03	37.73	-1.88	-1.72
	% diff of means	1.38		0.79		8.57	
5	A	2.88	2.84	42.40	41.10	-2.83	-2.68
	B	3.15	3.17	40.90	39.60	-2.44	-2.26
	C	2.94	2.90	34.20	34.20	-2.65	-2.44
	Mean	2.99	2.97	39.17	38.30	-2.64	-2.46
	% diff of means	0.67		2.21		6.90	
6	A	1.44	1.47	41.10	38.20	-4.64	-4.18
	B	2.15	2.19	55.60	54.80	-4.47	-3.97
	C	2.44	2.42	43.40	42.00	-4.62	-4.33
	Mean	2.01	2.03	46.70	45.00	-4.58	-4.16
	% diff of means	-1.00		3.64		9.08	
	Mean % diff of means	1.70		0.89		7.37	
	SD % diff of means	1.67		1.79		1.56	

^a It should be noted that region one of aerofoil T1 does not follow the expected trend of decreasing surface roughness with polishing. This was attributed to an issue in the parallel processing of aerofoils T1 and T2, but does not affect the analysis of the replication technique.

from the two data sets fall within a range of 0 mm to -0.143 mm discrepancy.

The mean of three chord profiles, taken towards the ends and middle of the aerofoil spans were averaged to

Table 2. Replication fidelity and repeatability in CCF_{max} and D_s for T1 and R1.

Quality	Mean region fidelity		Repeatability region 4	
	CCF_{max} (%)	D_s (%)	CCF_{max} (%)	D_s (%)
Parameter				
Mean	94.5	10.9	96.3	6.9
Standard deviation	0.8	2.8	0.7	1.7
Range	1.8	7.6	1.8	3.6

assess the cross sectional variation between the master and replica. Limited overall shrinkage was apparent in the replica, the shrinkage in mid chord thickness was approximately 140 μm or 2.5%. The maximum discrepancy for chord length was approximately 100 μm or 0.2%. This distribution of shrinkage is as anticipated as thicker sections are known to be more prone to shrinkage. It is less clear how warping might occur, though it may be related to which side the mould void is filled from and how the resin mixes upon filling.

3.4. Drag loss validation

The mean difference in drag coefficient between master and replicated regions of the tested aerofoils across a range of test flow conditions was less than 2%. This demonstrates that the aerodynamic performance of the replica aerofoil closely replicates that of titanium aerofoil for surfaces both above and below the admissible roughness level. This result validates the surface and geometric metrology results in showing that replication fidelity is high across all significant length scales.

3.5. Boundary layer transition by infrared thermography

Figure 12 shows a thermogram of the thermally insulating test aerofoil R1, it illustrates the aerodynamic technique for which the replication method detailed in the current paper was developed. Unlike the metallic test aerofoil T1 the resin aerofoil R1 is capable of supporting a temperature gradient sufficient to be captured by current thermal imaging systems, FLIR A315 [20] in this case.

Transition from laminar to turbulent flow is clearly visible as cooler dark regions of the aerofoil become lighter (warmer) under turbulent flow. As anticipated transition is only seen to occur at one of two sensitive locations, the aerofoil leading edge or close to peak suction (E-E). Peak suction is the aerofoil location where pressure is lowest and flow velocity is highest. In region (B) of the thermogram the highest levels of surface roughness on the aerofoil are seen to destabilise the laminar boundary layer and cause transition to turbulence at the leading edge. However transition in this region is not complete, flow is a combination of white 'turbulent wedges' from the leading edge and the remaining laminar flow becoming turbulent around peak suction. By this method, transition due to surface roughness can be expressed as a function of Reynolds

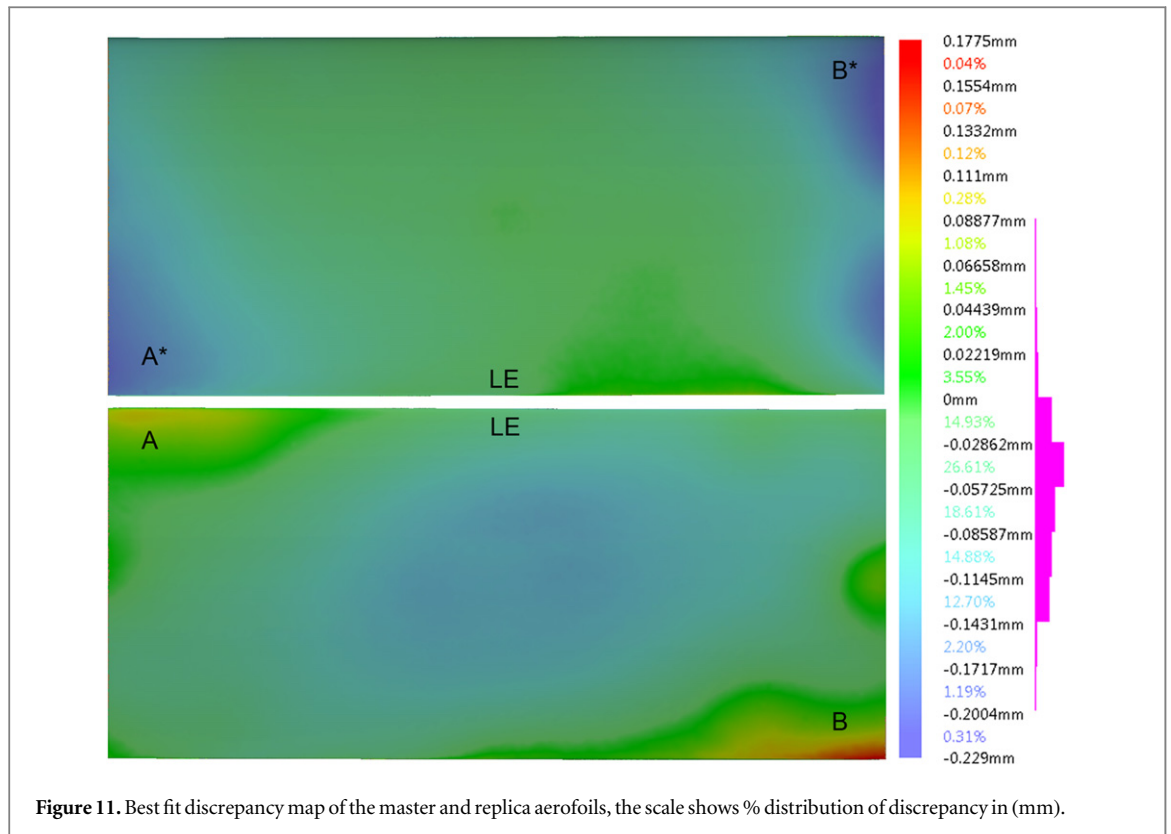


Figure 11. Best fit discrepancy map of the master and replica aerofoils, the scale shows % distribution of discrepancy in (mm).

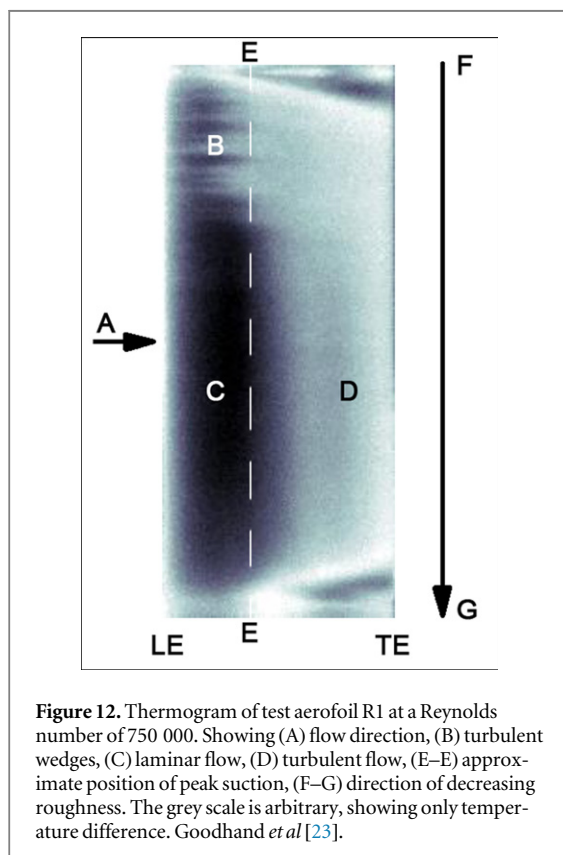


Figure 12. Thermogram of test aerofoil R1 at a Reynolds number of 750 000. Showing (A) flow direction, (B) turbulent wedges, (C) laminar flow, (D) turbulent flow, (E–E) approximate position of peak suction, (F–G) direction of decreasing roughness. The grey scale is arbitrary, showing only temperature difference. Goodhand *et al* [23].

number. Roughness induced drag data (as a function of Reynolds number) for aerofoil T1 can then be correlated with the transition data. This approach makes it possible to determine which of the two ‘roughness induced’ drag rise mechanisms (see section 3.1) causes the initial

drag rise over each roughness band on T1. As noted, these drag rise mechanisms are distinct and thus distinguishing between them is essential for meaningful modelling and data analysis.

4. Discussion

4.1. Replication technique

The slender geometry of the aerofoil and the requirement for an un-split mould meant that only the aerofoil ends were available for; mould filling, reinforcement, mounting and registration purposes. Thus pressurisation of both stages of replication helped improve filling of the high aspect ratio trailing edge and eliminate air bubbles in the casting resin. Given the specific requirements of the current casting process, a low viscosity, slow cure and low exotherm rigid casting was required with high fidelity surface roughness replication qualities. Polyurethane resin was found to fit these requirements well.

The selection of a low viscosity slow cure polyurethane resin blend also helped to offset these problems.

4.2. Metrology

Replication fidelity of the current technique is comparable to that reported for surface replication applications using mean areal field parameters as metrics. Though under the more exacting comparison of direct point height correlations the current method compares less well to an existing similar technique. Optimised values for CCF_{max} of 99% and D_s of 1% are reported for the

replication technique of Koch and Katterwe [7] and Song *et al* [10] which are significantly better than the values for the current method of 95% and 11% respectively. These parameters rely on precise alignment of the sample fields being compared and the technique adopted in the current paper was not specifically designed with this in mind. Thus parameter variation due to alignment error will contribute to any loss of fidelity. The technical difficulties inherent in the current technique may also adversely influence replication fidelity. Unlike the technique due to Koch and Katterwe [7] the current method combines high aspect ratios with significantly larger resin volume and fully enclosed casting. Thus poor dissipation of the heat generated during curing may contribute to the smooth surface replication artefact noted in figure 9 as this is not typically seen under optimal casting conditions.

4.3. Aerodynamic performance

Optimal infrared thermography results require a surface to have a uniformly high emissivity, meaning the surface should strongly and uniformly re-emit acquired thermal energy. The addition of black pigment to the polyurethane resin was found to satisfy this requirement.

5. Conclusions

The replication process, detailed in the current report, is geometrically accurate at all scales with variations in: Sa <2%, maximum aerofoil thickness ~2.5%, and drag loss <2%.

With the current technique replication fidelity is seen to decrease rapidly for the smoothest test surfaces. This is attributed to a high frequency surface artefact which may be the result of poor heat dissipation during curing.

The boundary layer transition behaviour due to surface roughness on a low conductivity resin test aerofoil surface can be determined using infrared thermography.

The accuracy in roughness replication means that the boundary layer transition location can be determined, combined with the accuracy in the aerofoil shape, this means that the aerofoil drag can be determined.

Further work is required to determine the cause of the reduced replication fidelity for the smoother surface in the current technique.

Acknowledgments

The authors gratefully acknowledge the funding and support of Rolls-Royce PLC.

The authors gratefully acknowledge the UK's Engineering and Physical Sciences Research Council (EPSRC) funding of the EPSRC Centre for Innovative Manufacturing in Advanced Metrology (Grant Ref: EP/I033424/1).

The authors would like to acknowledge the technical support of Nick Atkins and Will Playford.

References

- [1] Schlichting H and Gersten K 2000 *Boundary-Layer Theory* (Berlin: Springer)
- [2] Baals D D and Mourhess M J 1945 *Numerical Evaluation of the Wake-Survey Equations for Subsonic Flow Including the Effect of Energy Addition* DTIC Document
- [3] Tropea C, Yarin A L and Foss J F 2007 *Springer Handbook of Experimental Fluid Mechanics* vol 1 (Berlin: Springer)
- [4] Hansen H N, Hocken R J and Tosello G 2011 Replication of micro and nano surface geometries *CIRP Ann.—Manuf. Technol.* **60** 695–714
- [5] Nilsson L and Ohlsson R 2001 Accuracy of replica materials when measuring engineering surfaces *Int. J. Mach. Tools Manuf.* **41** 2139–45
- [6] Song J and Vorburger T 2006 Topography measurements and applications *3rd Int. Symp. on Precision Mechanical Measurements* (International Society for Optics and Photonics)
- [7] Koch A and Katterwe H 2007 Castings of complex stereometric samples for proficiency tests in firearm and tool mark examinations *AFTE J.* **39** 299–306
- [8] Akovali G 2001 *Handbook of Composite Fabrication* (Shrewsbury: Smithers Rapra)
- [9] Koch A 2005 Procedure to produce replicas of exact size and shape of complex stereometric bodies *Google Patents* (Germany) DE200510039823
- [10] Song J, Vorburger T V, Thompson R, Ballou S, Zheng A, Renegar T B, Silver R, Ols M, Wenz W and Koch A 2012 Topography measurements and performance comparisons between NIST SRM 2460 standard bullet masters and BKA bullet replicas *Forensic Sci. Int.* submitted for publication
- [11] Bergstrom T S, Brown C A, Hamel R A and Kummmail J J 2003 Tests for the fidelity of replicas in surface measurement *Scanning (J. Scanning Microsc.)* **25** 60–1
- [12] Microset 2014 *Product Index* Commercial page for Microset™, available from: <http://microset.co.uk/media/index.html>
- [13] Brumbach M T and Martinez R G 2011 *Evaluation of the Residue from Microset on Various Metal Surfaces* Sandia National Laboratories
- [14] EC Supplies 2014 *ECPU 3691 (Slow Cure) Polyurethane Resin* Retail web page, available from: <http://ecfbreglasssupplies.co.uk/p-2088-ecpu-3691-slow-cure-polyurethane-resin.aspx>
- [15] ISO_25178-606 2013 B.E., *BS EN ISO_25178-606 Draft Geometrical Product Specification (GPS) Surface Texture: Areal Part 606: Nominal Characteristics of Non-Contact (Focus Variation) Instruments* British Standards Institute
- [16] ISO_25178-3 2012 B.E., *BS EN ISO_25178-3 Geometrical Product Specifications (GPS) Surface Texture: Areal Part 3: Specification Operators* British Standards Institute
- [17] ISO_25178-2 2012 B.E., *BS EN ISO_25178-2 Geometrical Product Specifications (GPS) Surface Texture: Areal 2: Terms, Definitions and Surface Texture Parameters* British Standards Institute
- [18] Leach R E (ed) 2013 *Characterisation of Areal Surface Texture* (Berlin: Springer)
- [19] GOM 2015 *Product Index* 2015 Commercial page for GOM™, available from: <http://gom.com/>
- [20] FLIR 2014 *Manufacturer Data Sheet* 2014 Manufacturer data sheet, available from: <http://flir.com/cs/emea/en/view/?id=41955>
- [21] Thian S C H, Tang Y, Tan W K, Fuh J Y H, Wong Y S, Loh H T and Lu L 2008 The manufacture of micromould and microparts by vacuum casting *Int. J. Adv. Manuf. Technol.* **38** 944–8
- [22] Dassault_Systemes 2014 *Catia V5-6R2014*
- [23] Goodhand M N, Walton K, Blunt L, Lung H, Miller R J and Marsden R 2015 The limitations of 'Ra' to describe surface roughness *ASME Turbo EXPO 2015*